J Physiol 592.23 (2014) pp 5187–5202

The Journal of Physiology

Charge at the 46th residue of connexin 50 is crucial for the gap-junctional unitary conductance and transjunctional voltage-dependent gating

Xiaoling Tong[1], Hiroshi Aoyama[2], Tomitake Tsukihara[3,4] and Donglin Bai[1]

[1] *Department of Physiology and Pharmacology, Western University, London, Ontario, Canada*
[2] *Graduate School of Pharmaceutical Sciences, Osaka University, Osaka, Japan*
[3] *Institutes for Protein Research, Osaka University, Osaka, Japan*
[4] *Department of Life Science, University of Hyogo, 3-2-1 Koto, Kamighori, Akoh, Hyogo 678-1297, Japan*

Key points

- Gap-junction (GJ) channels provide direct intercellular communication and are twice the length of most membrane channels, yet they often have high efficiency in permeation of ions, which is reflected by large unitary channel conductance (γ_j).
- To reveal the key factors in determining the γ_j of a lens GJ channel, we studied connexin 50 mutant GJ channels, where a negatively or positively charged residue was introduced into a pore-lining domain.
- The results indicate that the pore surface electrostatic potential is a dictating factor for the connexin 50 GJ channel γ_j.
- A change in the local resistance of the channel pore associated with these mutant channels is an important factor for their voltage-dependent gating properties.
- The combination of dual patch clamp and homology structure modelling is a powerful approach in revealing molecular mechanisms of GJ gating and ion permeation.

Abstract Gap-junction (GJ) channels are twice the length of most membrane channels, yet they often have large unitary channel conductance (γ_j). What factors make this possibly the longest channel so efficient in passing ions are not fully clear. Here we studied the lens connexin (Cx) 50 GJs, which display one of the largest γ_j and the most sensitive transjunctional voltage-dependent gating (V_j gating) among all GJ channels. Introduction of charged residues into a putative pore-lining domain (the first transmembrane and the first extracellular loop border) drastically altered the apparent γ_j. Specifically, G46D and G46E increased the Cx50 γ_j from 201 to 256 and 293 pS, respectively and the G46K channel showed an apparent γ_j of only 20 pS. G46K also drastically altered V_j gating properties in homotypic G46K and heterotypic Cx50/G46K channels, causing an apparent loss of fast V_j-dependent gating transitions and leaving only loop gating transitions at the single channel current records. Both macroscopic and single channel currents of heterotypic Cx50/G46K channels showed a prominent rectification. Our homology structural models indicate that the pore surface electrostatic potentials are a dictating factor in determining the γ_j. Our data demonstrate, at the whole GJ channel level, a crucial role of the surface charge properties in the first transmembrane/first extracellular border domain in determining the efficiency of ion permeation and the V_j gating of Cx50 and possibly other GJ channels.

(Received 8 July 2014; accepted after revision 17 September 2014; first published online 25 September 2014)
Corresponding author D. Bai: Department of Physiology and Pharmacology, Western University, London, Ontario, N6A 5C1, Canada. Email: donglin.bai@schulich.uwo.ca

Abbreviations Cx50, connexin 50; E1, first extracellular domain; GJ, Gap-junction (channel); $G_{j,ss}$, normalized steady-state junctional conductance; γ_j, unitary channel conductance; I_j, macroscopic junctional current; i_j, single channel junctional current; TM1, the first transmembrane domain; V_j, transjunctional voltage.

DOI: 10.1113/jphysiol.2014.280636

Introduction

Gap-junction (GJ) channels allow direct intercellular exchange of ions and small signalling/metabolic molecules between neighbouring cells and play a key role in many physiological processes (Saez *et al.* 2003; Goodenough & Paul, 2009). GJ channels are oligomeric connexins of 21 different members (Sohl & Willecke, 2004; Goodenough & Paul, 2009), all of which with similar structural topology, including four transmembrane domains (TM1–TM4), two extracellular loops (E1 and E2), one cytoplasmic loop, with placement of both the amino terminus and carboxyl terminus in the cytosol (Simon & Goodenough, 1998; Saez *et al.* 2003; Sohl & Willecke, 2004). Six connexin molecules oligomerize to form a hemichannel and two hemichannels dock together at their extracellular domains to construct a whole GJ channel (a dodecamer of connexins). This unique structural arrangement of GJ channels makes them twice as long as most of the membrane channels and has probably the longest permeation passage for any membrane channels, yet the single channel conductance (γ_j) of a GJ channel can be as high as hundreds of picoSiemens (pS) in several homotypic GJs (Reed *et al.* 1993; Veenstra *et al.* 1994; Bukauskas *et al.* 1995; Srinivas *et al.* 1999). What makes the GJ channel so efficient in passing ions is not fully clear. One classical hypothesis believes that the pore diameter of a GJ channel with two docked hexameric hemichannels is much larger than the tetrameric or pentameric membrane channels that facilitate rapid ion permeation through the GJ channel (Hille, 2001). It is true that most GJ channels have a larger pore, allowing not only ions, but also other signalling/metabolic molecules up to 1 kDa to pass through. However, this model is unable to explain the well-documented experimental data that several large γ_j GJ channels showed a much lower cut-off size on permeable molecules than those GJ channels with much lower γ_j (Veenstra *et al.* 1995; Gong & Nicholson, 2013; Weber *et al.* 2004; Ek-Vitorin & Burt, 2005; Dong *et al.* 2006), indicating other pore properties may play an important role in facilitating ion permeation.

Experimental evidence is accumulated largely from hemichannel studies that the interface of TM1 and E1 domains (TM1/E1 border) probably forms part of the channel inner surface and plays a key role in determining the channel conductance of several connexins (Kronengold *et al.* 2003; Tang *et al.* 2009; Verselis *et al.* 2009), including Cx26 (Verselis *et al.* 1994; Sanchez *et al.* 2010, 2013). This structural prediction was confirmed by the high-resolution (at 3.5 Å) crystal structure of Cx26 GJ channel (Maeda *et al.* 2009). The amino acid residues at the TM1/E1 border form a narrow passage of the pore with a specialized helical structure [called 3(10) or parahelix for the residues of 42–51], which exposes several acidic residues toward the pore lumen forming a negatively charged path. Two such negatively charged enriched paths in each Cx26 GJ channel are believed to increase local cation concentration and facilitate the rate of cation permeation (Maeda *et al.* 2009). Several connexins, including Cx50, show high sequence identity and homology with Cx26, particularly at the TM1/E1 border domain, arguing that their GJ channels might have a similar structure and the negatively charged paths, which could play a role in the experimentally observed cation preference (Srinivas *et al.* 1999).

To study the role of the TM1/E1 border domain in the Cx50 GJ channel γ_j and transjunctional voltage-dependent gating (V_j gating) properties, we generated mutants with an additional negatively or positively charged residue in the middle of this domain (G46D/E and G46K). These mutations are predicted to decrease the pore size and to alter the surface electrostatic potentials in the negatively charged paths. Both G46D and G46E channels showed a significantly increased γ_j, while G46K channels substantially reduced the apparent γ_j. No fast gating and only loop gating was observed in homotypic G46K and heterotypic Cx50/G46K GJ channels. Our homology models indicate that the channel local surface electrostatic property of the GJ channel is an important factor to the rate of ion permeation. Changes in the channel local resistance at the TM1/E1 border domain by these mutants are probably responsible for the observed changes in V_j gating properties. Our data indicate that the pore surface charges at the TM1/E1 border domain of Cx50 channel are crucial for the γ_j and V_j gating properties.

Methods

Construction of connexin 50 mutants

Mouse Cx50 cDNA was obtained by polymerase chain reaction and was inserted into the pIRES2-EGFP vector. This Cx50 construct was used as a template for the point mutants, G46D, G46E and G46K. The QuikChange site-directed mutagenesis kit (Stratagene, La Jolla, CA, USA) was used to generate the mutants with following primers:

G46D Forward: 5′ GGAGTTTGTGTGGGACGATGAGCA ATC 3′
Reverse: 5′ GATTGCTCATCGTCCCACACAAACTCC 3′
G46E Forward: 5′ GCGGAGTTTGTGTGGGAGGATGAG CAATCTG 3′
Reverse: 5′ CAGATTGCTCATCCTCCCACACAAACTCC GC 3′
G46K Forward: 5′ GCGGAGTTTGTGTGGAAGGATGAG CAATCTG 3′
Reverse: 5′ CAGATTGCTCATCCTTCCACACAAACTCC GC 3′.

Cell culture and transient transfection

Mouse neuroblastoma (N2A) cells were purchased from American Type Culture Collection (ATCC, Manassas, VA, USA) and cultured with Dulbecco's modified Eagle's medium containing 10% fetal bovine serum. Before transfection, cells were plated in 35 mm dishes and the confluence was about 50% after overnight culture. Cx50 construct or mutant vector (1.5 μg) was transfected with 2 μl X-tremeGENE HP DNA Transfection Reagent (Roche Applied Sciences, Indianapolis, IN, USA). Cells were cultured for 24 h after transfection and replated on to glass coverslips ∼1–3 h before patch clamping recording.

When studying heterotypic Cx50/G46K GJs, Cx50 cDNA was carried in pcDNA3.1(–) expression vector and cotransfected with DsRed cDNA at a ratio of 4:1. G46K-IRES-GFP vector was transfected separately and the transfected cells were mixed with Cx50 and DsRed expressing cells to obtain heterotypic cell pairs. Only red/green cell pairs were chosen for patch clamp recording.

Electrophysiological recording

The V_j gating property of cell pairs expressing either Cx50 or its mutants was measured by dual whole cell voltage clamp technique as described earlier (Bai *et al.* 2006; Xin *et al.* 2010). Transfected cells were replated on glass coverslips with appropriate cell density for ∼1–3 h, transferred to a recording chamber on an inverted microscope (Leica DM IRB, Wetzlar, Germany) and then bathed in extracellular fluid at room temperature. The composition of the extracellular fluid is (in mM): 140 NaCl, 2 CsCl, 2 $CaCl_2$, 1 $MgCl_2$, 5 Hepes, 4 KCl, 5 D-glucose, 2 pyruvate, pH 7.2. Paired green fluorescent protein-positive cells were patched by two glass micropipettes (pipette resistance 2–5 MΩ), which were filled with intracellular fluid containing (in mM): 130 CsCl, 10 EGTA, 0.5 $CaCl_2$, 3 MgATP, 2 Na_2ATP, 10 Hepes, pH 7.2. Isolated cell pairs were selected and both of them were voltage clamped at 0 mV. The common protocol was that one cell of the pair was clamped at 0 mV while the apposed cell was administered with a series of voltage pulses from ±20 to ±100 mV in a 20 mV increment for a duration of 7 s. The junctional currents (I_j) were amplified with two Axopatch 200B amplifiers with a low-pass filter (cut-off frequency 1 kHz) and digitalized at 10 kHz sampling rate via an ADDA converter (Digidata 1322A; Molecular Devices, Sunnyvale, CA, USA).

For the ion preference experiment, the principal electrolyte in the intracellular fluid, CsCl, was replaced by equimolar tetraethylammonium chloride (TEACl) to eliminate/reduce the cation current (due to a much bulkier sized TEA^+ than Cs^+), or caesium glutamate (CsGlu) to diminish/reduce anion current (as the Glu^- is much larger than Cl^-). CsGlu solution was prepared by mixing equimolar CsOH with glutamic acid solution.

Homology structure modelling

The sequence of mouse Cx50 was aligned with that of Cx26 for the homology structure model. High sequence identity is observed in these two proteins (overall 49% and on the structure resolved part 57%). Cx26 crystal structure (2WZ3) (Maeda *et al.* 2009) was used as a template to replace residue by residue for the Cx50 structure. When a Cx50 residue replacement in the structure caused an abnormal inter-atomic contact, this was adjusted by hand initially in COOT and then revised by crystallography & NMR system energy refinement. After the energy refinement, structural validity of the model was inspected manually as described earlier (Nakagawa *et al.* 2011; Gong *et al.* 2001). Adaptive Poisson–Boltzman solver (Baker *et al.* 2001) and PDB2PQR server (http://nbcr-222.ucsd.edu/pdb2pqr_1.8/) were used to calculate the electron potentials of all atoms in the protein. The adaptive Poisson–Boltzman solver parameters were set as described previously (Maeda *et al.* 2009). PyMOL program was used for the diameter measurements and the structure presentations (DeLano, 2006).

Data analysis

To minimize the influence of series resistance on V_j gating properties, only those cell pairs with ≤5 nS junctional conductance (G_j) were selected for Boltzmann fitting analysis (Wilders & Jongsma, 1992). For each current trace, the normalized steady-state conductance ($G_{j,ss}$) was obtained by normalizing the steady-state current to the peak current. The dependence of $G_{j,ss}$ to positive or negative V_j was plotted and fitted with a two-state Boltzmann equation independently:

$$G_{j,ss} = (G_{max} - G_{min})/\{1 + \exp[A(V_j - V_0)]\} + G_{min}$$

V_0 is the voltage at which the conductance is reduced by half $[(G_{max} - G_{min})/2]$, G_{max} is the maximum normalized conductance, G_{min} is the normalized voltage insensitive residual conductance, and parameter A, describing the slope of the fitted curve, which reflects the V_j sensitivity of the GJ channels.

To record the single channel current, cell pairs with one or two operational channels were obtained by shortening the expression time after transfection. The amplitude of i_j was measured directly using Clampfit9 (Molecular Devices, Synnyvale, CA, USA) after digital filtering and plotted to corresponding V_j. The i_j–V_j plot was fitted by linear regression through the origin of the coordinates. The slope of the linear regression line is defined as the slope unitary conductance (γ_j).

The open (P_o), subconductance (P_s) or closed (P_c) probability represents the fraction of time that the channel

resides in the open, subconductance or closed state, respectively. To measure the P_o, P_s and P_c quantitatively in the Cx50 and G46D channels, the single channel currents during each of the V_j pulses were binned by their amplitude into all-point histograms to obtain the number of data points of each category (e.g. open/subconductance/closed state) separately, which is then divided by the total number of points.

To analyse single channel open dwell time, the single channel current records were digitally filtered at 500 Hz (Gaussian) and any events reaching half amplitude height and lasting >2 ms were considered as open events. The open events at the beginning and end of the V_j pulse were discarded, as the duration of these events was probably cut short by the V_j pulse. The dwell times of analysed events were binned into histograms and were fitted with two exponentials with time constants, τ_1 and τ_2, as described previously (Xin *et al.* 2010). τ_{mean} was calculated from the sum of the individual time constant with its weight.

Results

G46D formed functional gap-junction channels with similar transjunctional voltage gating properties as those of connexin 50

G46D was generated to increase the negative electrostatic surface potential in the middle of the TM1/E1 border domain of the GJ channel. Macroscopic transjunctional currents (I_j) in cell pairs expressing either Cx50 or G46D were obtained in response to the V_j pulses shown in Fig. 1*A*. The I_j of G46D-expressing cell pairs showed mirror symmetrical V_j-dependent inactivation when the absolute value of V_j was ≥40 mV. Normalized steady-state junctional conductance ($G_{j,ss}$) values from six cell pairs expressing either Cx50 or G46D were plotted against corresponding V_j and their Boltzmann fitted curves are almost identical to each other (Fig. 1*B* and Table 1), indicating that G46D has minor changes in macroscopic V_j gating properties.

G46D increased γ_j and the probability of the fully closed state, but decreased open dwell time

The single channel current (i_j) records of G46D GJ were obtained from cell pairs coupled with only one operational channel (Fig. 2*Ab*) and the channel properties are different from those of the Cx50 channels. First, the γ_j of G46D channel, estimated from a linear regression of i_j–V_j plots (Fig. 2*A* and *B*), was significantly increased to 256 ± 5 pS (n = 8) compared to Cx50 γ_j (201 ± 2 pS, n = 8, P < 0.001). Second, at the V_j of ±60 to ±80 mV, Cx50 channels showed few open events usually at the initial V_j pulses (Fig. 2*A*). Then, the channel dwelled almost exclusively in a subconductance state (Fig. 2*Aa*) and occasionally showed brief entries in the fully closed state (Fig. 2*Aa*, arrow). Similar to that of Cx50, the main open events of the G46D channel are usually clustered in the initial part of the V_j pulses. The subconductance states were also observed, but often with intermittent long-lived fully closed states (Fig. 2*Ab*, arrows). To quantify this observation, the probability of open (P_o), closed (P_c) and subconductance (P_s) states were measured and plotted to the V_j of ±60 and ±80 mV (Fig. 2*C*). The most significant changes of the G46D channel were the elevation of P_c, with a concurrent decrease in P_s (V_j ±80 mV) or an apparent decrease of both P_o and P_s (V_j ±60 mV). The significant increase in P_c in the G46D channels is probably due to an increased occurrence of loop gating, an increased stability of the fully closed state or combinations of both factors. Finally, as shown in Fig. 2*A*, the open dwell time

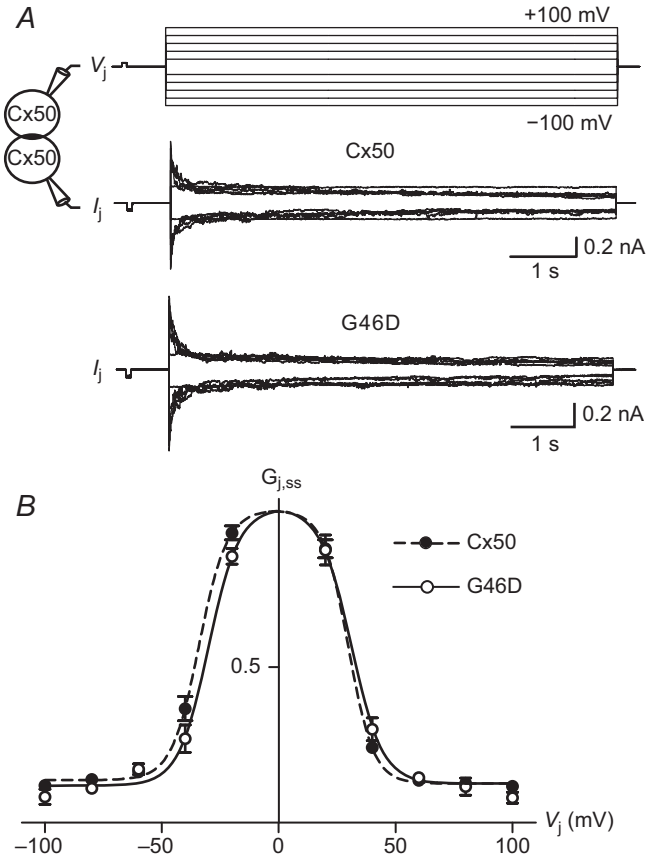

Figure 1. Macroscopic V_j gating properties of Cx50 G46D gap junction channels
A, V_j pulses from ±20 mV to ±100 mV in a 20 mV increment were applied to one cell of the cell pair expressing Cx50 or G46D and macroscopic transjunctional currents (I_j) recorded from the other cell are presented. *B*, normalized $G_{j,ss}$ of Cx50 (filled circles) and G46D (open circles) were plotted against different V_j. Smooth dash and continuous lines represent best fitting curves of averaged data from Cx50 (n = 6) and G46D (n = 6) channels, respectively, to a two-state Boltzmann function. Cx50, connexin 50.

Table 1. Boltzmann fitting parameters for connexin 50 (Cx50) and its mutants

	V_j polarity	G_{min}	V_0	A
Cx50	+	0.13 ± 0.01	29.8 ± 0.8	0.18 ± 0.01
	−	0.14 ± 0.01	33.6 ± 1.0	0.16 ± 0.02
G46D	+	0.13 ± 0.02	31.1 ± 1.5	0.15 ± 0.02**
	−	0.12 ± 0.02	30.0 ± 1.2***	0.15 ± 0.02
G46E	+	0.11 ± 0.01**	28.1 ± 0.8**	0.17 ± 0.01
	−	0.11 ± 0.01***	28.8 ± 0.8***	0.19 ± 0.02*
G46K	+	0.55 ± 0.09***	50.7 ± 10.4***	0.05 ± 0.04***
	−	0.60 ± 0.06***	53.4 ± 6.9***	0.05 ± 0.02***
Cx50/G46K	+	0.07 ± 0.14	28.1 ± 17.5	0.04 ± 0.02***

Data are presented as means ± S.E.M. and V_0 are absolute values. Student's t test was used to compare the Boltzmann fitting parameters of the mutants against those of the wild-type Cx50 with the same V_j polarity. The number of asterisks indicate the statistical difference level (*$P < 0.05$, **$P < 0.01$, ***$P < 0.001$).

for the G46D channel appeared to be shorter than that of Cx50. This was measured systematically in several V_j (Fig. 2*D*). In these V_j for both the G46D and Cx50, the open dwell times displayed two time constants (τ_1 and τ_2) with various distributions. The weighted average open dwell time (τ_{mean}) for G46D was getting shorter with the increase in V_j values from ±40 mV (77 ms), to ±60 mV (44 ms) to ±80 mV (19 ms). In all V_j, the τ_{mean} of the G46D channel was shorter than the corresponding ones of Cx50 (Fig. 2*D*), indicating that the open state of the G46D channel is less stable and easier to transfer to a subconductance or fully closed state at these V_j.

G46E channel showed higher γ_j than that of G46D

Increased γ_j of the G46D channel is surprising because the side chain of Asp (D) is much larger than that of Gly (G). The G46D mutation is predicted to decrease the physical pore size at the 46th position. However, introduction of a negatively charged residue might alter the local pore surface electrostatic properties, which could play a role in facilitating the ion permeation through this cation-preferring channel (Srinivas *et al.* 1999). To test this hypothesis further, we generated another mutant, G46E, in which Gly (G) was replaced by another negatively charged residue Glu (E) with a longer side chain than Asp (D). As shown in Fig. 3*A*, macroscopic I_j in response to the same V_j pulses were similar to those observed in the Cx50 channels. $G_{j,ss}$–V_j plots of the G46E channel were nicely fitted by Boltzmann equations in both V_j polarities and the fitted curves are virtually identical to those of Cx50 (Table 1).

At the single channel level, the γ_j of G46E channel, generated by the i_j–V_j plot, was 293 ± 4 pS, $n = 4$, which is nearly 50% larger than that of Cx50 (Fig. 3*B*). It is also significantly larger than that of G46D ($P < 0.001$). The i_j showed a long-lived fully closed state in the tested V_j (Fig. 3*C*, arrows). Measurements from two cell pairs yielded the following probabilities in each state (P_o, P_s and P_c) at V_j of ±60 mV (0.04, 0.42 and 0.54) and ±80 mV (0.02, 0.19 and 0.79), respectively, similar to those observed in G46D channels. A temporal expansion of a cluster of open events under 80 mV V_j indicates that G46E channel also showed a shorter open dwell time (all of the open events are shorter than 40 ms) than that of the Cx50 channel (with a τ_{mean} of 68 ms at this V_j). In summary, the characteristics of the G46E channel seem to resemble those of G46D at both macroscopic and single channel levels. The only exception is that G46E produced an even larger γ_j than G46D.

G46K channel showed much lower γ_j and an altered V_j gating

Introduction of a negatively charged residue at the TM1/E1 border, G46D/E, drastically increased γ_j. To explore the effects of introducing a positively charged residue into this domain, G46K was generated. Different from those of Cx50, the I_j of the G46K channel showed little V_j-dependent inactivation in the range of ±40 mV. Higher values of V_j (±60 to ±100 mV) produced a moderate level of inactivation (Fig. 4*A*). The $G_{j,ss}$–V_j plot and the associated Boltzmann fitting curves of G46K channels were drastically different from those of Cx50 (Fig. 4*B*). Multiple Boltzmann fitting parameters of G46K channel were changed, including larger G_{min} and decreased V_j gating sensitivities (Table 1).

The unitary channel currents (i_j) were only discernible at large V_j (±80 mV or larger) due to the low apparent γ_j of G46K. An all-point histogram was generated for a portion of i_j at the 80 mV V_j and was fitted by two Gaussian functions to obtain the γ_j (Fig. 4*C*). The average apparent γ_j of the G46K channel was 20 ± 1 pS ($n = 3$), which was only about 10% of the Cx50 γ_j. A representative i_j record at V_j of 80 mV depicted a prolonged

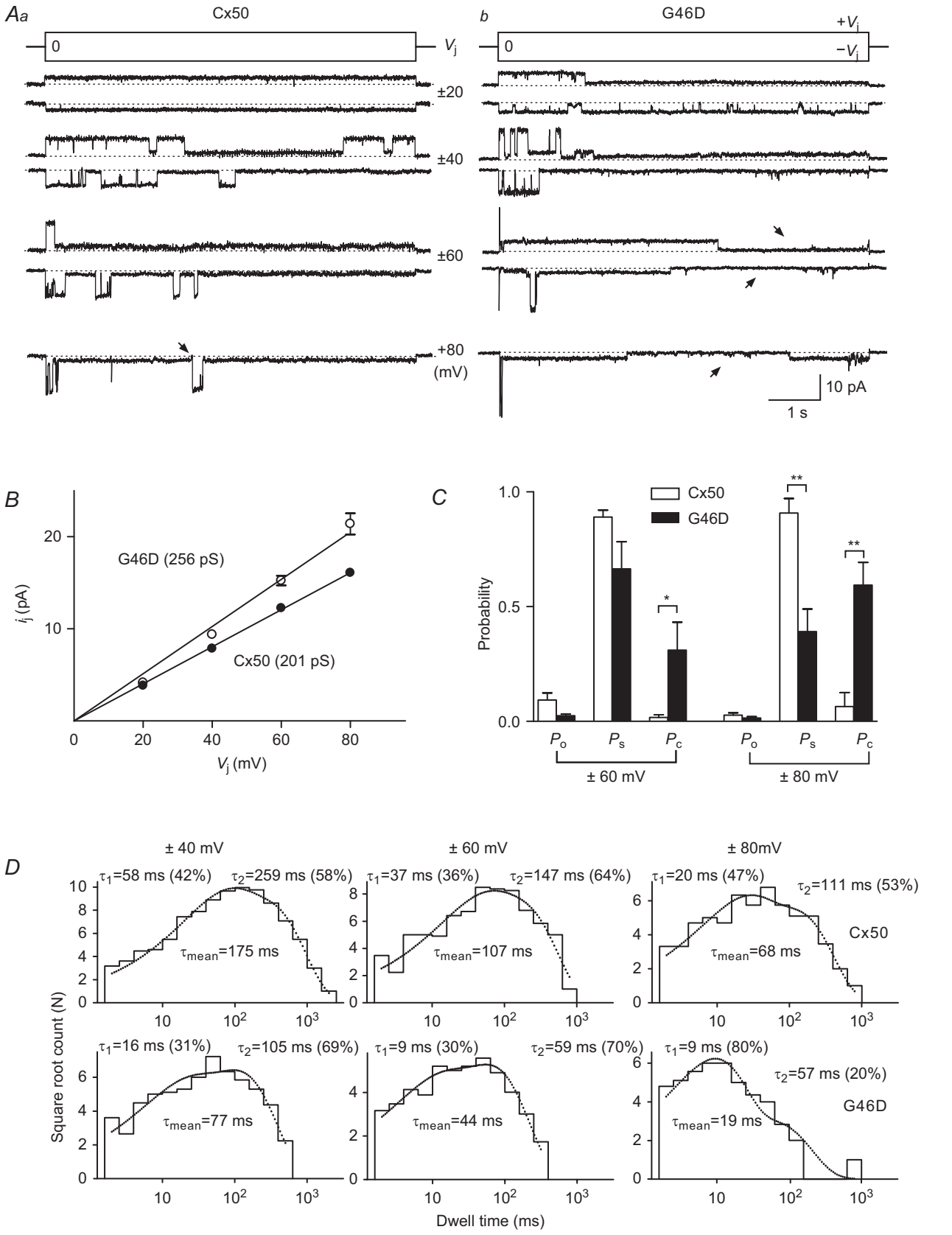

Figure 2. G46D alters single channel properties

open dwell time for each event with occasional transitions to a closed/subconductance state (Fig. 4*C*). Open probability (P_o) at this V_j was higher than that of the Cx50 channel ($P_o = 0.03$, see Fig. 2*C*). Even at a much higher V_j (120 mV), the G46K channel resided mostly at an open state initially and then the channel was fully closed (Fig. 4*D*). The gating transitions were very slow, usually took tens of milliseconds or longer (Fig. 4*D*), indicating the transitions are probably loop gating.

Heterotypic connexin 50/G46K channels displayed asymmetric V_j gating and current rectification

The G46K V_j gating properties are drastically different from those of Cx50 and could be interpreted because of the impairment of the fast gate. To test this further, we studied the V_j gating of heterotypic Cx50/G46K channels, in which the docked Cx50 hemichannel is known to have a fast gate (with positive gating polarity) and a loop gate (with a negative gating polarity) (White *et al.* 1994; Hopperstad *et al.* 2000). When applying the Cx50-expressing cell with $+V_j$ (or the G46K cell with $-V_j$), the recorded I_j showed apparent V_j-dependent inactivation (Fig. 5*A*). Conversely, administrating $-V_j$ to the Cx50-expressing cells (or $+V_j$ to the G46K-expressing cell) did not cause any perceptible current inactivation (Fig. 5*A*). The V_j gating process during the $+V_j$ on the Cx50 side was nicely fitted by Boltzmann equation (Fig. 5*B*). A significantly reduced gating sensitivity (Fig. 5*A*) was observed, while other Boltzmann parameters are similar to those of the Cx50 channels (Table 1).

It is noted that the initial amplitude of the I_j was larger when the Cx50-expressing cell was applied with $+V_j$ than those corresponding I_j with $-V_j$ (Fig. 5*A*), indicating that the heterotypic Cx50/G46K channels possess a rectifying property. To quantify this, the initial conductance ($G_{j,ini}$) at each $+V_j$ and $-V_j$ was measured, and then the ratio of $G_{j,ini}(+)/G_{j,ini}(-)$ was calculated and plotted to V_j (Fig. 5*C*). A significant V_j-dependent rectification was revealed in the high V_j (60–100 mV; Fig. 5*C*) on the heterotypic Cx50/G46K GJs. No rectification was observed on the homotypic Cx50 GJs, as the ratios of $G_{j,ini}(+)/G_{j,ini}(-)$ were close to 1 (Fig. 5*C*).

Single heterotypic connexin 50/G46K channel showed asymmetric γ_j and only slow gating transitions

Figure 5*D* illustrates i_j of a heterotypic Cx50/G46K channel in response to V_j. When the holding potential of the Cx50-expressing cell was relatively negative to the G46K cell ($-V_j$), stable i_j were recorded with minimum transitions to any other states. However, when the Cx50-expressing cells were applied with $+V_j$, the channel was initially open and then flickered with frequent transitions between the closed/subconductance states and multiple levels of open states; later the channel settled at either a subconductance or a closed state (Fig. 5*D*). A temporal expansion of a portion of i_j revealed that the transition time typically required tens of milliseconds or longer (Fig. 5*D*), indicating these transitions are probably loop gatings. Surprisingly, we did not observe any fast gating transitions when the Cx50 hemichannel side was applied with positive V_j (which is predicted to occur from a positive V_j gating polarity of the Cx50 channel). A simple interpretation of these data is that G46K increased the local resistance for ion permeation (see below for details) on the G46K hemichannel side of the heterotypic channel and the V_j was redistributed (more on the G46K hemichannel side) leading to an increase in loop gating in the G46K hemichannel, which would cause flickering channel activities and later fully close the channel. This was supported by the fact that these slow gating transitions only occurred when the G46K cell was under $-V_j$.

Parallel to the finding on the initial macroscopic junctional conductance, the γ_j also showed strong rectification on this heterotypic channel. The $\gamma_j(+)$, defined as the γ_j when the Cx50 cell was applied with $+V_j$, was measured as 54 pS (Fig. 5*E*). Meanwhile, the $\gamma_j(-)$ (when the Cx50 cell was applied with $-V_j$) was only 22 pS (Fig. 5*E*). The average data from four different heterotypic cell pairs yielded apparent $\gamma_j(+)$ of 50 ± 4 pS and $\gamma_j(-)$ of 24 ± 5 pS ($n = 4$, $P < 0.001$). Apparently, these γ_j values of Cx50/G46K channels are much lower than the γ_j of the homotypic Cx50 junction channel (201 ± 2 pS), but closer to the γ_j of the homotypic G46K channel (20 ± 1 pS), implying that the G46K hemichannel is probably the dominant rate-limiting part of this heterotypic channel.

A, representative single channel current records of Cx50 channel (*Aa*) and G46D channel (*Ab*) are illustrated in response to different V_j as indicated. Single channel currents of G46D displayed a shortened dwell time of most open events at different V_j and long-lived fully closed state (indicated by arrows in *Ab*) in response to ±60 mV and +80 mV pulses. Only one brief transition to closed state was observed in Cx50 channel (arrow in *Aa*). Dotted lines indicate the fully closed current level. *B*, average single channel slope conductance (γ_j) of G46D channel ($n = 8$) was much higher than that of Cx50 ($n = 8$, $P < 0.001$). *C*, P_o, P_s and P_c represent the probabilities of the channel in open, subconductance and fully closed state, respectively. Bar graph illustrates the average data from four different cell pairs. Number of asterisks above the bar indicates the level of statistical difference (*$P < 0.05$, **$P < 0.01$). G46D channel demonstrated a markedly increased P_c at these V_j. *D*, open dwell time of G46D channel is shorter than that of Cx50. Dotted lines are the Gaussian fit of a two-term exponential function to the histograms. Time constants τ_1 and τ_2 with their relative weight are shown. τ_{mean} is the mean open dwell time obtained from the sum of the product of each τ and its relative weight. τ_1, τ_2 and τ_{mean} are all reduced in G46D channel. Cx50, connexin 50.

G46D failed to alter the ion preference of the connexin 50 channel

A previous study indicates that Cx50 channels preferentially permeate cations over anions (Srinivas *et al.* 1999). Introduction of an extra negatively charged residue in the pore-lining domain (TM1/E1 border) of each subunit in the channel, such as G46D, would be predicted to have an increase in negative surface charges (six for each hemichannel and 12 for each GJ channel). This substantial increase in the surface negative charge is predicted to have electrostatic effects on the ions passing through the channel, leading to a possibly higher/lower local cation/anion concentrations, respectively. To test this hypothesis, we studied the γ_j of the G46D channel with an increased size of the major conducting cations (from Cs^+ to TEA^+) or anions (from Cl^- to Glu^-). Much larger sized

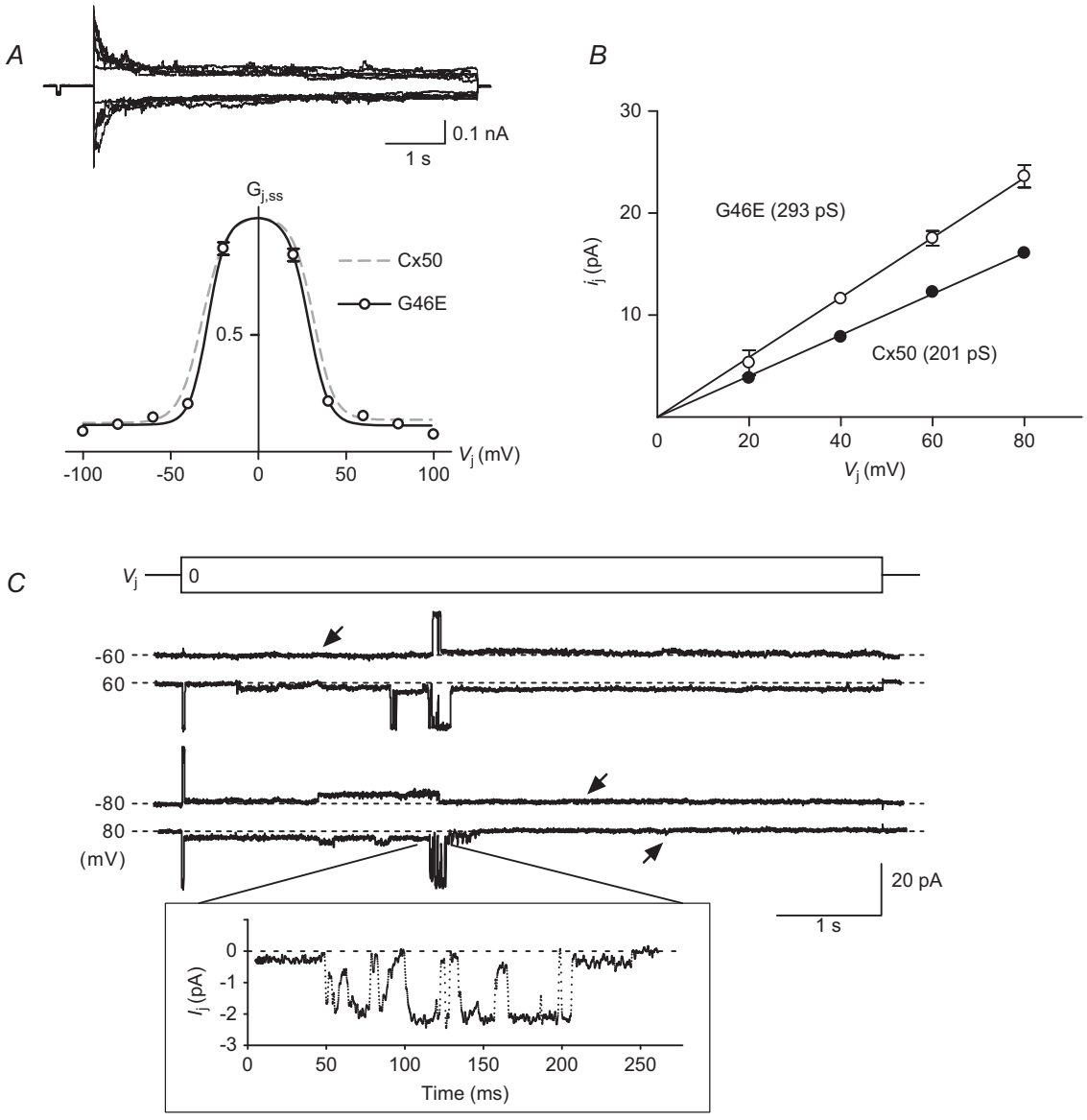

Figure 3. Macroscopic and single channel properties of G46E GJs
A, macroscopic junctional currents (I_j) of homotypic G46E channels are shown in response to the same V_j as shown in Fig. 1*A*. $G_{j,ss}$–V_j relationships of G46D were constructed ($n = 6$) and were fitted to Boltzmann functions. Fitting curves of Cx50 (grey dashed lines) are obtained from Fig. 1*B* for comparison. *B*, linear regression of i_j–V_j plots showed an increased γ_j of G46E channel [$n = 4$, $P < 0.001$ *vs.* Cx50 (same as shown in Fig. 2*B*)]. *C*, single channel current traces of G46E channel under the indicated V_j showed the existence of the fully open state, subconductance state and fully closed state. Arrows point to the long-lived fully closed state. Temporal expanded trace (inset) with multiple openings indicates that the open dwell times in these open events were short. Cx50, connexin 50.

TEA^+ or Glu^- was used to amplify the ionic preference of the channel.

As predicted, the Cx50 channel showed only a minor reduction (9%) in the γ_j when the major electrolyte CsCl was changed to CsGlu (Fig. 6*A* and *B*; 183 ± 2 pS, $n = 4$, $P < 0.001$) and a major reduction (80%) in the γ_j when the CsCl was changed to TEACl (41 ± 2 pS, $n = 4$, $P < 0.001$), demonstrating indeed that the Cx50 channel has a strong cation preference. However, the G46D channel showed a nearly identical proportional increase (about a quarter) in the γ_j using each of the salt solutions compared to those of Cx50 (Fig. 6*A* and *B*), CsCl (256 ± 5 pS, $n = 8$), CsGlu (228 ± 5, $n = 4$, $P < 0.001$) and TEACl (57 ± 1 pS, $n = 4$, $P < 0.001$), while maintaining the same percentage decrease in the γ_j (11% in CsGlu and 78% in TEACl), indicating that G46D increased ion permeation without a substantial change in the channel preference on cations.

Similar ion preferential experiments were also used to test if the G46K GJ channel displays a reduced cation preference. Using the CsGlu-based pipette solution, we were able to identify i_j in two cell pairs with γ_j of 5 and 8 pS of more than 40 cell pairs (data not shown). The γ_j (with CsGlu) is much lower than that in CsCl (20 ± 1 pS, $n = 4$), indicating the G46K channel did show a decrease in the cation preference. However, as it is very difficult to obtain enough data for quantitative comparisons, this observation should be regarded as preliminary. None of the G46K cell pairs showed distinguishable unitary channel currents with the TEACl pipette solution, suggesting either the γ_j is too small to be resolved under the experimental conditions or the channel does not have a stable open state.

Homology models of the connexin 50, G46D, G46E and G46K channels

Most connexins have a very high sequence homology with human Cx26, including mouse Cx50 used in the present study. The sequence identity on the crystal structure resolved domains of Cx26 and Cx50 proteins is high (57%), which is sufficient for generating a homology structural model. The initial model of the Cx50 homomeric homotypic channel was generated by using the coordinates of the crystallized Cx26 channel (Maeda *et al.* 2009). The homology model was then adjusted to eliminate contacts and minimized in energy terms similar to our previous studies (Nakagawa *et al.* 2011; Gong *et al.* 2001). The homology models were developed without the knowledge of the experimental results.

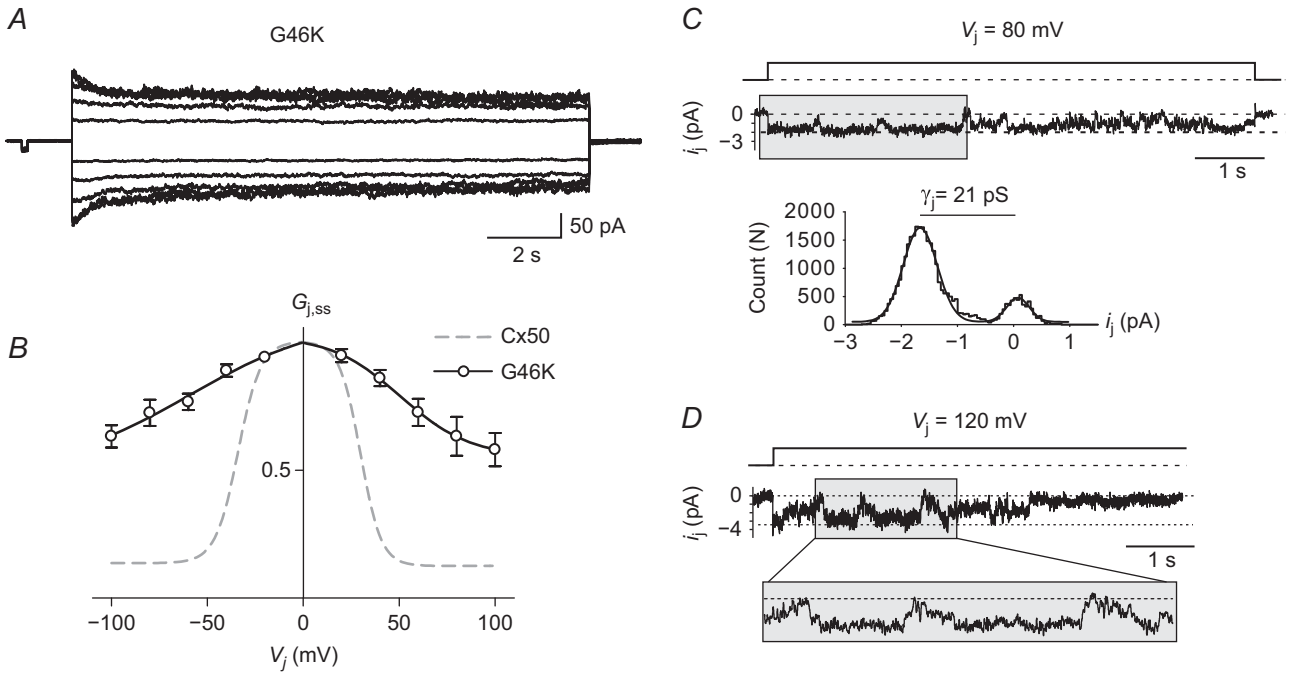

Figure 4. G46K displays drastically altered V_j gating and single channel properties
A, a set of macroscopic I_j traces of G46K GJs in response to V_j of ±20 ~ ±100 mV. *B*, Boltzmann fitting curves of G46K GJs (continuous lines) generated from $G_{j,ss}$–V_j plots ($n = 6$) exhibited lower V_j sensitivities than those of Cx50 GJs (grey dashed lines, same as in Fig. 1*B*). *C*, single channel current (i_j) of a G46K channel at 80 mV V_j showed a very low unitary conductance (21 pS). Closing and opening current levels are indicated by dotted lines. Despite the frequent transfer to closed state, the dominant state of G46K channel is open state at this V_j. *D*, i_j of a G46K channel at 120 mV V_j showed slow transitions between open and closed states. A portion of the trace is expanded in temporal domain. Cx50, connexin 50; GJ, gap-junction.

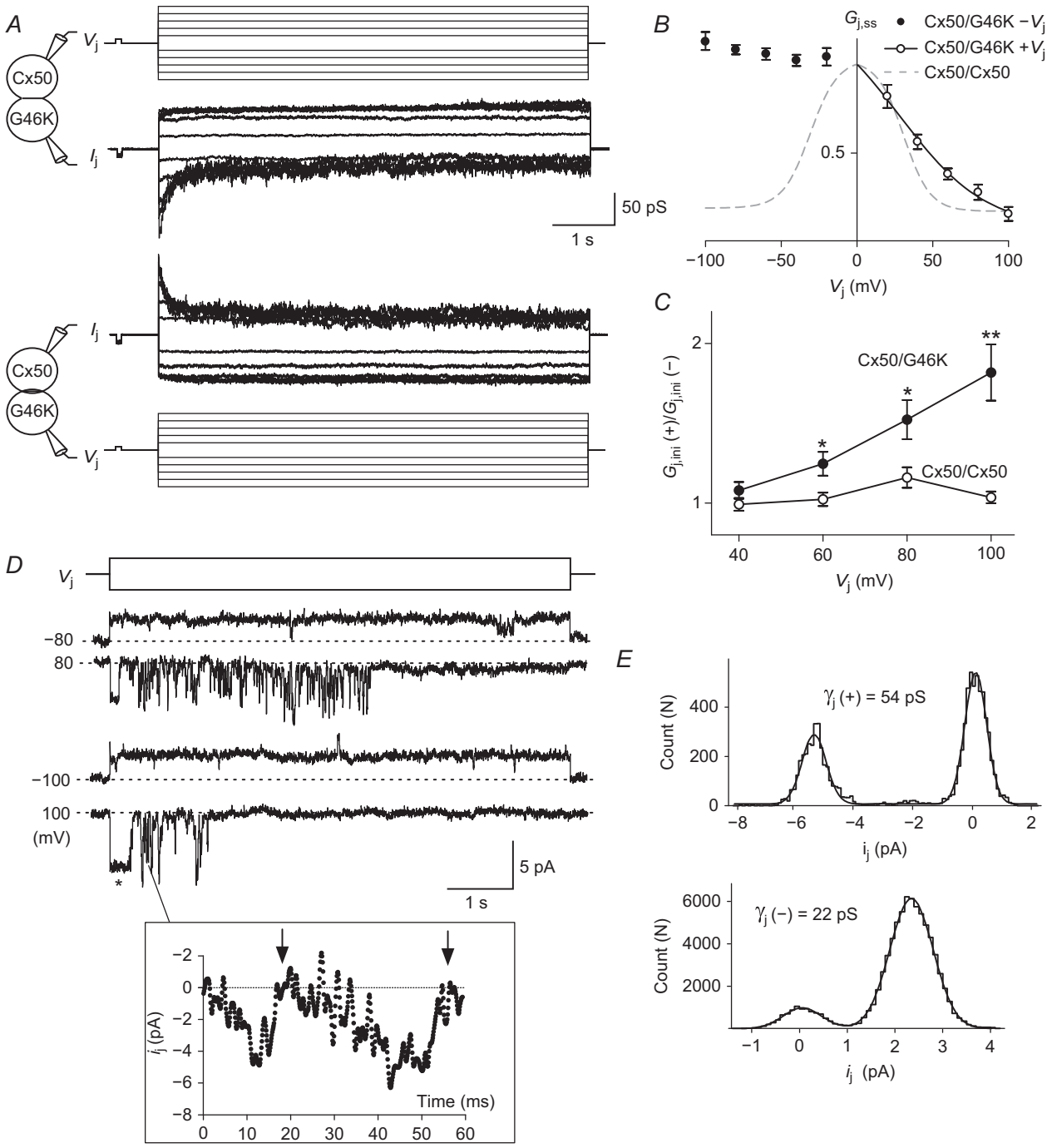

Figure 5. Heterotypic Cx50/G46K channels show asymmetrical V_j gating and rectification
A, two sets of representative I_j of heterotypic Cx50/G46K GJs in response to the V_j protocol (±20 to ±100 mV) applied to the Cx50-expressing cell (top set) or to the G46K-expressing cell (bottom set). I_j inactivations were present only when the Cx50 cell with $+V_j$ (or the G46K cell with $-V_j$). Initial amplitudes of I_j were also different between the corresponding $+V_j$ and $-V_j$. *B*, $G_{j,ss}$–V_j plot of heterotypic Cx50/G46K GJs from six cell pairs. Smooth line on the $+V_j$ is the Boltzmann fitting curve. At the $-V_j$, no V_j gating (I_j inactivation) was evident. Boltzmann fittings of Cx50 channels (grey dashed lines) are shown for comparison. *C*, initial conductance of $+V_j$ [$G_{j,ini}(+)$] and $-V_j$ [$G_{j,ini}(-)$] were calculated and the ratio is plotted with V_j. Cx50/G46K GJs showed a strong V_j-dependent rectification. *D*, heterotypic Cx50/G46K channel showed rectification. i_j was recorded from the G46K cell in response to ±80 mV and ±100 mV V_j pulses (on the Cx50-expressing cell). As indicated in the enlarged box below the current, the gating closure reached the fully closed state (indicated by arrows) and the gating transitions typically took tens of milliseconds. *E*, when the Cx50 cell with $+V_j$, the $\gamma_j(+)$ was 54 pS (from the i_j portion indicated by an asterisk). $\gamma_j(-)$ with $-V_j$ was 22 pS. Cx50, connexin 50; GJ, gap-junction.

The homology model of Cx50 displayed many similar structural properties with that of the crystal structure of Cx26, including the TM1/E1 border domains forming a narrow part of the pore. The homology structures for the G46D, G46E and G46K mutants of Cx50 revealed two important structural changes: (1) the channel pore diameter at this position was estimated to be decreased from 20.6 Å for Cx50 to 17.1 Å for G46D, 12.6 Å for G46E and 11.4 Å for G46K on each of the docked hemichannels (Fig. 7*A*) (a reduction in pore diameter could constrict the total number of ions in this part of the pore and lead to much closer interactions between the passing ions and inner surface residues), and (2) these mutants displayed a drastic change in the electrostatic potentials at the TM1/E1 border of the channel. As shown in Fig. 7*B*, both G46D and G46E substantially increased the local negativity of electrostatic potential, while G46K created a local narrow ring of positive electrostatic potential at this domain (Fig. 7*B*). Both the reduced diameter and the ring of positive electrostatic potential in G46K channel could increase the resistance of the channel to ions and electrostatically reduce the local cation concentration, respectively. The latter effect is also predicted to increase the resistance of this cation-preferring channel. Our experimental data on the γ_j changes associated with these mutants indicate that the channel inner surface charge properties are a dominant factor in determining the γ_j of the Cx50 channel.

Increased local positive electrostatic potential might create a local electrostatic barrier for permeating cations and substantially decrease the γ_j of the G46K channel. In the heterotypic Cx50/G46K channel, the asymmetrical electrostatic potentials in the two docked hemichannels are predicted to contribute to the observed channel rectification. To explore the possible factors leading to the V_j-dependent rectification of the heterotypic Cx50/G46K channel (Fig. 5), we inspected the homology structure model of G46K. The Lys46 (K46) residue contains a long and flexible side chain with a positively charged amino group at the end. These properties of Lys enable multiple orientations in response to V_j polarity and intensity. As shown in two possible models with either $+V_j$ or $-V_j$ (Fig. 7*C*), the pore sizes at the Lys46 (K46) position are

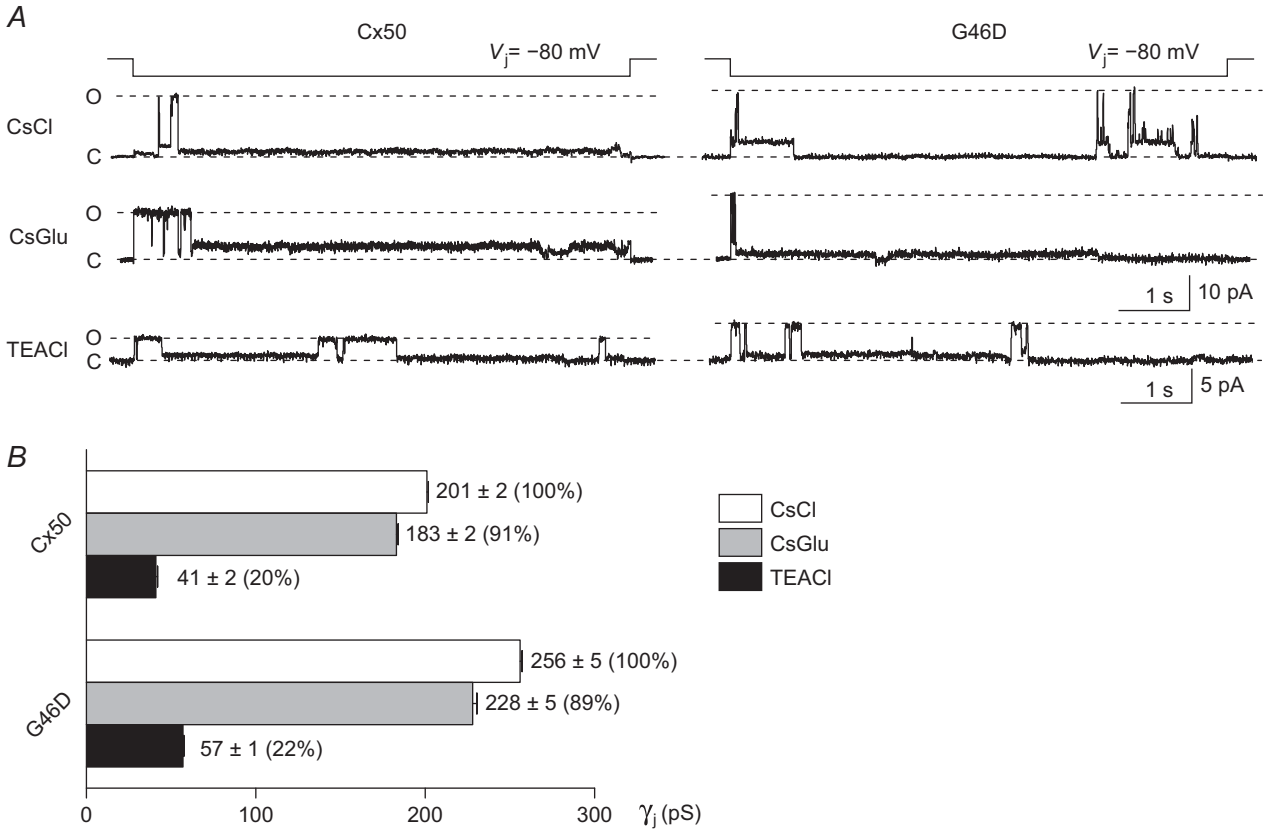

Figure 6. G46D channel show a similar ion preference as that of Cx50
A, with the substitutions of the major salt (either from CsCl to CsGlu or to TEACl) in the pipette solution, single channel recordings of Cx50 and G46D GJ displayed distinctive γ_j. i_j in response to V_j of −80 mV were shown for each of the ion substitutions. *B*, bar graph shows the average of the γ_j of Cx50 and G46D while using different pipette solutions and their ratios to the control γ_j (using CsCl-based pipette solution). All the γ_j values were obtained by linear regression of i_j–V_j plots. CsGlu, caesium glutamate; Cx50, connexin 50; TEACl, tetraethylammonium chloride.

different, which could play a role in the observed current rectification of the γ_j of the heterotypic Cx50/G46K channels. At present we could not rule out that other structural changes might also occur with these mutants, which could provide alternative interpretations to our experimental data.

Discussion

The present study describes the effects of introducing a negatively/positively charged residue (D, E or K) into the TM1/E1 border domain on the macroscopic and unitary channel properties of the Cx50 GJ channels. G46D/E channel showed little change in the macroscopic V_j gating properties, but significantly increased the γ_j and the probability of the channel residing in the fully closed states, while G46K channel displayed drastic changes in both the V_j gating properties and the apparent γ_j. Heterotypic Cx50/G46K channels showed strong rectification in both macroscopic and single channel currents. Our homology models indicate that these mutations could change the pore electrostatic properties of the GJ channel, leading to an altered local resistance for the major permeating ions (cations) and the relative V_j distributions across the whole length of the channel. Altered V_j distribution in the channel in turn could cause apparent changes in fast gating and loop gating properties in these mutants. The charge substitutions in the TM1/E1 border domain were shown to drastically change the γ_j from nearly 300 pS (G46E) to an apparent 20 pS (G46K), demonstrating the crucial roles of this domain in determining γ_j and V_j gating properties of the Cx50 GJ channel. Distinct from most of the previous studies on undocked hemichannels, our study focused on characterizations of whole GJ channels without any pharmacological manipulations.

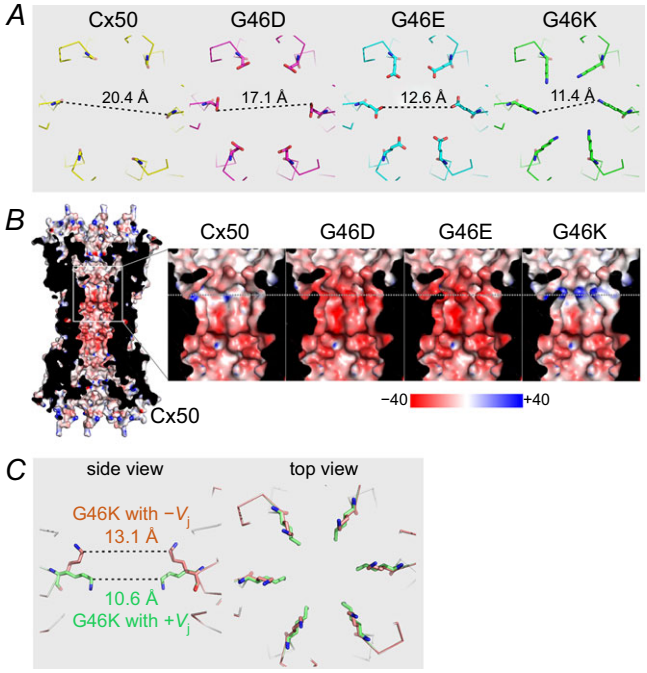

Figure 7. Homology models of the Cx50 mutants
A, stick view in PyMOL of a portion of the mutant or wild-type Cx50 channels near the 46th residue (top view). Estimated diameters of G46D, G46E and G46K were predicted to decrease as indicated. *B*, side view of a cut open Cx50 channel shows the pore surface electrostatic potentials (calculated with an adaptive Poisson–Boltzman solver) using dielectric constants of 2 (protein) and 80 (solutions) (Baker *et al.* 2001). A portion of the Cx50 channel pore surface containing TM1/E1 domains are enlarged as indicated. Electrostatic potentials of the mutant channels at the same position are illustrated. Drastic differences in electrostatic potentials are observed near the mutant residue (dotted horizontal line). Displayed surface electrostatic potentials range from −40 (red) to +40 (blue) kTe^{-1}. *C*, when the G46K-expressing cell was held with different polarity of V_j, two different orientations of Lys46 could be observed and are superimposed in stick view in PyMOL. G46K channel with $-V_j$ (or Cx50 side with $+V_j$ in the heterotypic channel) showed a larger diameter than the G46K channel with $+V_j$, which could play a role in channel rectification. Cx50, connexin 50.

Factors determining the γ_j in the mutants

Crucial factors for the ion permeation (the γ_j) through GJ channels are not fully resolved. Here we studied the Cx50 GJ channel with γ_j (200 pS), one of the largest among all characterized GJs (Srinivas *et al.* 1999; Bai *et al.* 2006; Gonzalez *et al.* 2007; Xin & Bai, 2013). Mutations on the Gly46 to long side-chained and charged residues (G46D, G46E and G46K) all probably decrease the pore size and alter electrostatic properties. However, the γ_j were actually substantially increased for both G46D (more than a quarter higher) and G46E (almost 50% higher) from the Cx50 channel. This result has several implications. First, it is improbable that the pore size variations of these mutant channels could reach any substantial steric hindrance to ion permeation, while the pore surface electrostatic properties could substantially facilitate ion permeation, similar to those described in BK channels (Brelidze *et al.* 2003; Geng *et al.* 2011). Considering that the Cx50 channel is a cation-preferring channel, adding $6 \times 2 = 12$ additional negatively charged residues (D or E) in the permeation path would be expected to increase the negativity of the electrostatic potential as shown in Fig. 7, perhaps to facilitate further the accumulation of local cations and reduction of anions for permeation. However, our data on the γ_j changes with an enlarged cation (TEA^+) or anion (Glu^-) failed to demonstrate a change in the estimated relative permeability for cations over anions, at least for the G46D channel. We also do not know the mechanism for an even higher γ_j on the G46E channel than that of G46D. Perhaps the longer side chains of Glu46 in the pore increase the local negative charge density and/or they are more flexible, both of which

could favour ion permeation. Second, the native Cx50 GJ channel is not fully optimized in its ability to pass ions. A single mutation, G46E, made this large γ_j channel even larger and almost equal to the largest γ_j of all GJ channels, the Cx37 channel (Reed *et al.* 1993; Veenstra *et al.* 1994; Traub *et al.* 1998). Detailed comparison of the pore-lining residues and their properties of large γ_j channels *versus* low γ_j GJ channels may help us to understand more about the ion permeation of these important channels. Understanding the factors controlling ion permeation can offer new avenues for engineering GJs with enhanced channel function, which can be useful in improving/re-establishing the GJ function in many disease-linked connexin mutants (Lee & White, 2009; Beyer *et al.* 2013; Bai, 2014). Third, the positively charged residue at the same position, G46K, substantially reduced the apparent γ_j to 1/10 of the Cx50. We believe that this again was mainly due to the change of surface electrostatic potentials and the local charge density of a ring of Lys^+ residues in the pore. A narrow positively charged ring in the G46K channel is predicted to repel cations and reduce the local cation concentration, which can reduce the γ_j of this cation-preferring channel. In addition to this, a substantial reduction in the pore size and the increase in positive charge density locally might also contribute to the reduced γ_j. Another possible explanation for the low apparent γ_j of G46K could be that what we recorded is the subconductance state of the mutant GJ channel not the fully open state. However, the apparent γ_j of G46K was much lower than the conductance of the main subconductance state in the Cx50 channel and we never observed a higher unitary conductance level (similar to that of the Cx50 main conductance state) in any of our unitary channel records of homotypic G46K channels and heterotypic Cx50/G46K channels. Finally, the heterotypic Cx50/G46K channel showed a strong rectification in γ_j. This prompted us to look into the potential structural basis. Lys (K) has a positively charged amino group ($-NH_3^+$) at the end of a long flexible side chain. V_j changes could provide sufficient energy to drive the positively charged amino group to different orientations. Our homology modelling showed that when under different V_j, the side chain of Lys could move to different positions in the pore causing a reduction/enlargement of the diameter and possibly the pore surface electrostatic potentials. This could be a simple explanation of the observed rectification of the heterotypic Cx50/G46K channel. Obviously, it is too early to rule out the possibility that other structural changes could also play a role in the observed rectification.

V_j-dependent loop gating was increased in G46D and virtually exclusive in G46K gap-junction channels

Previous studies showed that the Cx50 displayed little loop gating in both hemichannel and GJ channel recordings (Srinivas *et al.* 1999, 2005). Consistent with these early findings, our data on the Cx50 single channel currents rarely display loop gating transition to the fully closed state. When these rare gating events did happen, they were very brief, usually less than a fraction of a second. However, G46D (and G46E) channels showed an increased incidence of loop gating and substantially prolonged the dwell time in the fully closed state, which significantly increased the probability of the channel in the closed state. The increased stability of the closed state was accompanied by a reduced stability of the open and subconductance state, particularly during the high V_j. When the V_j were at $\pm$100 mV a portion of G46D (and G46E) channels dwelled in the fully closed state at the end of the V_j pulse, making the data of the macroscopic $G_{j,ss}$–V_j plot consistently below the fitting curves.

Different from what was observed in G46D/E, the G46K channels drastically changed the macroscopic V_j gating properties. V_j gating was virtually eliminated, which was well described by the changes in Boltzmann parameters: G_{min} were more than 4-fold higher and A values were reduced to $\sim$1/3 of those of Cx50 channels. Studies on the single G46K channel revealed a substantially reduced γ_j, which is probably due to the mutation that created an electrical barrier for the permeating ions at the TM1/E1 border of the pore. Such an electrical barrier (increase in resistance) is expected to increase the V_j drop across this region of the GJ pore, causing V_j redistribution, which could increase the sensitivity of the loop gating sensor and decrease sensitivity of the fast gating sensor. Such a model can also be used to explain our data on the heterotypic Cx50/G46K channels, where the K46 position on the mutant hemichannel would have the highest resistance of the entire GJ channel, which would not only dictate the γ_j, but also receive the majority of the V_j. In addition, this redistribution of the V_j would reduce the V_j drop on the sensors controlling the fast gates of both the Cx50 and G46K hemichannels, causing an apparent loss of the fast gates in these heterotypic GJ channels. This model is a simple plausible interpretation of our experimental data.

The first transmembrane/first extracellular border domain is a hotspot for human disease-linked mutations

Mutations in several connexin genes are linked to inherited human diseases, including cataract (Cx50 and Cx46) (Beyer *et al.* 2013) and non-syndromic and syndromic deafness (Cx26) (Lee & White, 2009). Many of these mutants are clustered around the TM1/E1 domain (Lee & White, 2009; Beyer *et al.* 2013), indicating that the residues at this domain are important for normal GJ functions in these connexins. Several mutants are directly on the G46 (or equivalent) residues. G46R and G46V of the Cx50 were

found linked to cataract (Minogue *et al.* 2009; Sun *et al.* 2011). An *in vitro* expression study on G46V revealed that this mutant caused cell death possibly due to increased hemichannel activities (Minogue *et al.* 2009). In Cx26, G45E (equivalent to G46 in Cx50) was found linked to the keratitis–ichthyosis–deafness syndrome (Janecke *et al.* 2005; Griffith *et al.* 2006). In the *in vitro* expression system, the G45E was expressed at a similar level as wild-type Cx26 and formed a similar level of GJ coupling (Gerido *et al.* 2007). However, the V_j gating properties of G45E channels were changed (decrease in the V_0) (Gerido *et al.* 2007; Sanchez *et al.* 2010) and the single hemichannel conductance was increased by ∼25% (Sanchez *et al.* 2010). The increase in the single hemichannel conductance of G45E is consistent with our finding; however, we did not observe any obvious change in the V_j gating properties in either G46E or G46D, indicating that either the V_j gating sensor and/or the V_j distribution in the Cx50 channel are probably different from those of Cx26. Whether these biophysical property changes of Cx26-G45E contribute to the disease burden are not fully resolved, but could be an additive factor to the proposed key disease-causing mechanism, the increase in hemichannel function (Stong *et al.* 2006; Gerido *et al.* 2007; Sanchez *et al.* 2010; Mese *et al.* 2011).

Structure–function study of the connexin 50 G46 equivalent residues in other connexins

Early studies identified that the TM1/E1 border domain lines the GJ pore, which plays important roles in normal physiological functions, such as gating and Ca^{2+} sensing, and mutations at this domain are associated with serious diseases (Verselis *et al.* 1994; Oh *et al.* 1999; Trexler *et al.* 2000; Gomez-Hernandez *et al.* 2003; Janecke *et al.* 2005; Griffith *et al.* 2006; Minogue *et al.* 2009). A detailed systematic mapping of all the residues around this domain was carried out on Cx46 hemichannels and found that the Gly46 is one of the crucial residues in determining the single hemichannel conductance. Similar to our findings on the Cx50 GJ channels, introducing a positively charged residue [such as Lys, Arg or Cys with modifications by positively charged methanethiosulphonates (MTS)] at this position substantially reduced the single hemichannel conductance (Kronengold *et al.* 2003). However, the introduction of a negatively charged residue by the G46C mutation with modification by a negatively charged MTS (ES^-) in the Cx46 hemichannel did not increase the single hemichannel conductance (Kronengold *et al.* 2003), possibly due to the fact that the MTS-ES^- on Cys is much larger than the Glu^- or Asp^- side chain (making the channel smaller) or that Cx46 could be a much less cation-preferring channel compared to Cx50. Consistent with our findings on the altered γ_j of Cx50 mutants, Cx26-G45C showed qualitative similar hemichannel conductance changes after reacting to positively or negatively charged MTS reagents (Sanchez *et al.* 2010). Hemichannel studies on Cx26-G45E or equivalent mutants in Cx26, Cx30, Cx32 and Cx43 have shown the importance of this position to extracellular Ca^{2+}-dependent closure of these hemichannels (Sanchez *et al.* 2010; Zhang & Hao, 2013). These studies and our results argue a significant role for the TM1/E1 border domain in the biophysical GJ channel properties.

References

Bai D (2014). Atrial fibrillation-linked GJA5/connexin40 mutants impaired gap junctions via different mechanisms. *FEBS Lett* **588**, 1238.

Bai D, del Corsso C, Srinivas M & Spray DC (2006). Block of specific gap junction channel subtypes by 2-aminoethoxydiphenyl borate (2-APB). *J Pharmacol Exp Ther* **319**, 1452–1458.

Baker NA, Sept D, Joseph S, Holst MJ & McCammon JA (2001). Electrostatics of nanosystems: application to microtubules and the ribosome. *Proc Natl Acad Sci U S A* **98**, 10037–10041.

Beyer EC, Ebihara L & Berthoud VM (2013). Connexin mutants and cataracts. *Front Pharmacol* **4**, 43.

Brelidze TI, Niu X & Magleby KL (2003). A ring of eight conserved negatively charged amino acids doubles the conductance of BK channels and prevents inward rectification. *Proc Natl Acad Sci U S A* **100**, 9017–9022.

Bukauskas FF, Elfgang C, Willecke K & Weingart R (1995). Biophysical properties of gap junction channels formed by mouse connexin40 in induced pairs of transfected human HeLa cells. *Biophys J* **68**, 2289–2298.

DeLano WL (2006). The PyMOL Molecular Graphics System. v.0.99.

Dong L, Liu X, Li H, Vertel BM & Ebihara L (2006). Role of the N-terminus in permeability of chicken connexin45.6 gap junctional channels. *J Physiol* **576**, 787–799.

Ek-Vitorin JF & Burt JM (2005). Quantification of gap junction selectivity. *Am J Physiol Cell Physiol* **289**, C1535–1546.

Geng Y, Niu X & Magleby KL (2011). Low resistance, large dimension entrance to the inner cavity of BK channels determined by changing side-chain volume. *J Gen Physiol* **137**, 533–548.

Gerido DA, DeRosa AM, Richard G & White TW (2007). Aberrant hemichannel properties of Cx26 mutations causing skin disease and deafness. *Am J Physiol Cell Physiol* **293**, C337–345.

Gomez-Hernandez JM, de Miguel M, Larrosa B, Gonzalez D & Barrio LC (2003). Molecular basis of calcium regulation in connexin-32 hemichannels. *Proc Natl Acad Sci U S A* **100**, 16030–16035.

Gong XQ, Nakagawa S, Tsukihara T & Bai D (2013). A mechanism of gap junction docking revealed by functional

rescue of a human-disease-linked connexin mutant. *J Cell Sci* **126**, 3113–3120.

Gong XQ & Nicholson BJ (2001). Size selectivity between gap junction channels composed of different connexins. *Cell Commun Adhes* **8**, 187–192.

Gonzalez D, Gomez-Hernandez JM & Barrio LC (2007). Molecular basis of voltage dependence of connexin channels: an integrative appraisal. *Prog Biophys Mol Biol* **94**, 66–106.

Goodenough DA & Paul DL (2009). Gap junctions. *Cold Spring Harb Perspect Biol* **1**, a002576.

Griffith AJ, Yang Y, Pryor SP, Park HJ, Jabs EW, Nadol JB, Jr., Russell LJ, Wasserman DI, Richard G, Adams JC & Merchant SN (2006). Cochleosaccular dysplasia associated with a connexin 26 mutation in keratitis-ichthyosis-deafness syndrome. *Laryngoscope* **116**, 1404–1408.

Hille B (2001). *Ion Channels of Excitable Membrane*. Sinauer Associates, Inc., Sunderland, MA.

Hopperstad MG, Srinivas M & Spray DC (2000). Properties of gap junction channels formed by Cx46 alone and in combination with Cx50. *Biophys J* **79**, 1954–1966.

Janecke AR, Hennies HC, Gunther B, Gansl G, Smolle J, Messmer EM, Utermann G & Rittinger O (2005). GJB2 mutations in keratitis-ichthyosis-deafness syndrome including its fatal form. *Am J Med Genet A* **133A**, 128–131.

Kronengold J, Trexler EB, Bukauskas FF, Bargiello TA & Verselis VK (2003). Single-channel SCAM identifies pore-lining residues in the first extracellular loop and first transmembrane domains of Cx46 hemichannels. *J Gen Physiol* **122**, 389–405.

Lee JR & White TW (2009). Connexin-26 mutations in deafness and skin disease. *Expert Rev Mol Med* **11**, e35.

Maeda S, Nakagawa S, Suga M, Yamashita E, Oshima A, Fujiyoshi Y & Tsukihara T (2009). Structure of the connexin 26 gap junction channel at 3.5 Å resolution. *Nature* **458**, 597–602.

Mese G, Sellitto C, Li L, Wang HZ, Valiunas V, Richard G, Brink PR & White TW (2011). The Cx26-G45E mutation displays increased hemichannel activity in a mouse model of the lethal form of keratitis-ichthyosis-deafness syndrome. *Mol Biol Cell* **22**, 4776–4786.

Minogue PJ, Tong JJ, Arora A, Russell-Eggitt I, Hunt DM, Moore AT, Ebihara L, Beyer EC & Berthoud VM (2009). A mutant connexin50 with enhanced hemichannel function leads to cell death. *Invest Ophthalmol Vis Sci* **50**, 5837–5845.

Nakagawa S, Gong XQ, Maeda S, Dong Y, Misumi Y, Tsukihara T & Bai D (2011). Asparagine 175 of connexin32 is a critical residue for docking and forming functional heterotypic gap junction channels with connexin26. *J Biol Chem* **286**, 19672–19681.

Oh S, Rubin JB, Bennett MV, Verselis VK & Bargiello TA (1999). Molecular determinants of electrical rectification of single channel conductance in gap junctions formed by connexins 26 and 32. *J Gen Physiol* **114**, 339–364.

Reed KE, Westphale EM, Larson DM, Wang HZ, Veenstra RD & Beyer EC (1993). Molecular cloning and functional expression of human connexin37, an endothelial cell gap junction protein. *J Clin Invest* **91**, 997–1004.

Saez JC, Berthoud VM, Branes MC, Martinez AD & Beyer EC (2003). Plasma membrane channels formed by connexins: their regulation and functions. *Physiol Rev* **83**, 1359–1400.

Sanchez HA, Mese G, Srinivas M, White TW & Verselis VK (2010). Differentially altered Ca^{2+} regulation and Ca^{2+} permeability in Cx26 hemichannels formed by the A40V and G45E mutations that cause keratitis ichthyosis deafness syndrome. *J Gen Physiol* **136**, 47–62.

Sanchez HA, Villone K, Srinivas M & Verselis VK (2013). The D50N mutation and syndromic deafness: altered Cx26 hemichannel properties caused by effects on the pore and intersubunit interactions. *J Gen Physiol* **142**, 3–22.

Simon AM & Goodenough DA (1998). Diverse functions of vertebrate gap junctions. *Trends Cell Biol* **8**, 477–483.

Sohl G & Willecke K (2004). Gap junctions and the connexin protein family. *Cardiovasc Res* **62**, 228–232.

Srinivas M, Costa M, Gao Y, Fort A, Fishman GI & Spray DC (1999). Voltage dependence of macroscopic and unitary currents of gap junction channels formed by mouse connexin50 expressed in rat neuroblastoma cells. *J Physiol* **517**, 673–689.

Srinivas M, Kronengold J, Bukauskas FF, Bargiello TA & Verselis VK (2005). Correlative studies of gating in Cx46 and Cx50 hemichannels and gap junction channels. *Biophys J* **88**, 1725–1739.

Stong BC, Chang Q, Ahmad S & Lin X (2006). A novel mechanism for connexin 26 mutation linked deafness: cell death caused by leaky gap junction hemichannels. *Laryngoscope* **116**, 2205–2210.

Sun W, Xiao X, Li S, Guo X & Zhang Q (2011). Mutational screening of six genes in Chinese patients with congenital cataract and microcornea. *Mol Vis* **17**, 1508–1513.

Tang Q, Dowd TL, Verselis VK & Bargiello TA (2009). Conformational changes in a pore-forming region underlie voltage-dependent 'loop gating' of an unapposed connexin hemichannel. *J Gen Physiol* **133**, 555–570.

Traub O, Hertlein B, Kasper M, Eckert R, Krisciukaitis A, Hulser D & Willecke K (1998). Characterization of the gap junction protein connexin37 in murine endothelium, respiratory epithelium, and after transfection in human HeLa cells. *Eur J Cell Biol* **77**, 313–322.

Trexler EB, Bukauskas FF, Kronengold J, Bargiello TA & Verselis VK (2000). The first extracellular loop domain is a major determinant of charge selectivity in connexin46 channels. *Biophys J* **79**, 3036–3051.

Veenstra RD, Wang HZ, Beblo DA, Chilton MG, Harris AL, Beyer EC & Brink PR (1995). Selectivity of connexin-specific gap junctions does not correlate with channel conductance. *Circ Res* **77**, 1156–1165.

Veenstra RD, Wang HZ, Beyer EC, Ramanan SV & Brink PR (1994). Connexin37 forms high conductance gap junction channels with subconductance state activity and selective dye and ionic permeabilities. *Biophys J* **66**, 1915–1928.

Verselis VK, Ginter CS & Bargiello TA (1994). Opposite voltage gating polarities of two closely related connexins. *Nature* **368**, 348–351.

Verselis VK, Trelles MP, Rubinos C, Bargiello TA & Srinivas M (2009). Loop gating of connexin hemichannels involves movement of pore-lining residues in the first extracellular loop domain. *J Biol Chem* **284**, 4484–4493.

Weber PA, Chang HC, Spaeth KE, Nitsche JM & Nicholson BJ (2004). The permeability of gap junction channels to probes of different size is dependent on connexin composition and permeant-pore affinities. *Biophys J* **87**, 958–973.

White TW, Bruzzone R, Wolfram S, Paul DL & Goodenough DA (1994). Selective interactions among the multiple connexin proteins expressed in the vertebrate lens: the second extracellular domain is a determinant of compatibility between connexins. *J Cell Biol* **125**, 879–892.

Wilders R & Jongsma HJ (1992). Limitations of the dual voltage clamp method in assaying conductance and kinetics of gap junction channels. *Biophys J* **63**, 942–953.

Xin L & Bai D (2013). Functional roles of the amino terminal domain in determining biophysical properties of Cx50 gap junction channels. *Front Physiol* **4**, 373.

Xin L, Gong XQ & Bai D (2010). The role of amino terminus of mouse Cx50 in determining transjunctional voltage-dependent gating and unitary conductance. *Biophys J* **99**, 2077–2086.

Zhang Y & Hao H (2013). Conserved glycine at position 45 of major cochlear connexins constitutes a vital component of the Ca^{2+} sensor for gating of gap junction hemichannels. *Biochem Biophys Res Commun* **436**, 424–429.

Additional information

Competing interests

Authors declare no conflict of interests.

Author contributions

X.T. designed and performed all patch clamp experiments; analysed data and wrote an early draft of the manuscript. H.A. and T.T. performed homology modelling and wrote relevant part of the manuscript. D.B. designed the project, supervised data analysis and critically revised the manuscript.

Funding

This work was supported by a grant to D.B. from Natural Sciences and Engineering Research Council of Canada. This work was also supported by Grants-in-Aid for Scientific Research (16087206, 18207006 and 21227003 to T.T. and 26440029 to H.A.) from the Ministry of Education, Culture, Sports, Science and Technology of Japan.

Acknowledgements

We thank Dr Brian Shilton for helpful discussions on an earlier version of the manuscript.